Jumping the Gap: Searching for LIGO's Biggest Black Holes

Jose María Ezquiaga[1,3] and Daniel E. Holz[1,2]

[1] Kavli Institute for Cosmological Physics and Enrico Fermi Institute, The University of Chicago, Chicago, IL 60637, USA; ezquiaga@uchicago.edu
[2] Department of Physics, Department of Astronomy & Astrophysics, The University of Chicago, Chicago, IL 60637, USA

Abstract

Gravitational wave (GW) detections of binary black holes (BBHs) have shown evidence for a dearth of component black holes with masses above $\sim 50 M_\odot$. This is consistent with expectations of a mass gap due to the existence of pair-instability supernovae (PISN). We argue that ground-based GW detectors will be sensitive to BBHs with masses above this gap, $\gtrsim 120\,M_\odot$. With no detections, 2 yr at upgraded sensitivity (A+) would constrain the local merger rate of these BBHs on the "far side" of the PISN gap to be lower than $0.01\,\mathrm{yr}^{-1}\mathrm{Gpc}^{-3}$. Alternatively, with a few tens of events we could constrain the location of the upper edge of the gap to the percent level. We consider the potential impact of "interloper" black holes within the PISN mass gap on this measurement. Far side BBHs would also be observed by future instruments such as Cosmic Explorer (CE), Einstein Telescope (ET) and LISA, and may dominate the fraction of multiband events. We show that by comparing observations from ground and space it is possible to constrain the merger rate history. Moreover, we find that the upper edge of the PISN mass gap leaves an imprint on the spectral shape of the stochastic background of unresolved binaries, which may be accessible with A + sensitivity. Finally, we show that by exploiting the upper edge of the gap, these high-mass BBHs can be used as standard sirens to constrain the cosmic expansion at redshifts of ~ 0.4, 0.8, and 1.5 with LISA, LIGO-Virgo, and CE/ET, respectively. These far-side binaries would be the most massive BBHs LIGO-Virgo could detect.

Unified Astronomy Thesaurus concepts: Gravitational waves (678); Astrophysical black holes (98)

1. Introduction

The first three observing runs of Advanced LIGO (The LIGO Scientific Collaboration et al. 2015) and Virgo (Acernese et al. 2014) have shown evidence for a population of stellar-mass binary black holes (BBHs) with a dearth of masses above $\sim 50\,M_\odot$ (Fishbach & Holz 2017; Abbott et al. 2019a, 2019b, 2020a). This is consistent with pair-instability supernova (PISN; Barkat et al. 1967; Fowler & Hoyle 1964; Heger & Woosley 2002; Fryer et al. 2001; Heger et al. 2003; Belczynski et al. 2016), a runaway process induced by electron–positron pair production occurring in massive stars. These PISN result in complete disruption of the stars, preventing the formation of remnant black holes and thus inducing a gap in the mass spectrum. However, for sufficiently massive stars the PISN process is insufficient to prevent direct collapse, and a population of intermediate mass black holes (IMBHs) with masses above $\sim 120 M_\odot$ is expected to arise. IMBHs have been a long-standing target of the LIGO Virgo Collaboration (LVC; Abadie et al. 2012; Aasi et al. 2014; Abbott et al. 2019c), and firm upper bounds have been set on their merger rate with O1-O2 data (Abbott et al. 2019c).

These "far side" or "post gap" massive binaries appear in a range of formation channels. For example, they may be produced in field binaries (Madau & Rees 2001; Belczynski et al. 2014; Marchant et al. 2016; Mangiagli et al. 2019) or in globular clusters (Giersz et al. 2015; Rodriguez et al. 2016). Still, the PISN gap may not be strictly empty, since it could be partially filled with black holes from second generation mergers in dense star clusters (Fishbach et al. 2017; Gerosa & Berti 2017, 2019; Rodriguez et al. 2019) and galactic nuclei (Yang et al. 2019), stellar collisions (Di Carlo et al. 2019), quadruple systems (Fragione et al. 2020), or gas accretion (Roupas & Kazanas 2019). However, existing data show that only $2^{+3.4}_{-1.7}\%$ of BBH systems have primary masses

above $45\,M_\odot$ (Abbott et al. 2020a), robustly demonstrating a precipitous drop in the BBH population above $45\,M_\odot$. The fact that the population shows this drop is in some sense a strong validation of theoretical predictions of a PISN feature at precisely this location in the mass distribution.

The LVC has recently announced GW190521 (Abbott et al. 2020b), the most massive binary detected thus far. Under uninformative priors, GW190521 shows evidence for both the primary and secondary masses being located within the PISN gap (Abbott et al. 2020c). By assuming a population informed prior in which the secondary mass is considered a member of the O1+O2 population distributions, Fishbach & Holz (2020a) have shown that the primary mass could instead be the first black hole on the far side of the PISN gap. Of course, this is not a definitive determination, but it further motivates our consideration of a far-side, post-PISN population.

BBHs above the PISN mass gap would be extraordinarily loud sources of GWs. Remarkably, these binaries lie at the intersection of ground- and space-based detector sensitivities, complementing stellar-mass multiband binaries (Sesana 2016). In this Letter we study the sensitivity of present and future detectors to the mergers of far-side binaries. We explore a range of gap locations and population properties, as well as different instruments. We address the precision with which the end of the gap could be constrained, both from the detection of individual sources and from the stochastic background of unresolved sources. We also propose the use of the edge of the mass gap to directly constrain the cosmic expansion rate using standard sirens at high redshift. Detecting this new population of black holes would have important implications for astronomy, fundamental physics, and cosmology.

The potential existence of "interloper" binaries within the gap does not invalidate the existence of a PISN mass gap. These may be members of a subpopulation due to a completely different formation channel, such as hierarchical mergers. Nevertheless, as

---

[3] NASA Einstein fellow.

we discuss further below, current observations allow for a significant population of BBHs above the gap. Despite evidence for BBHs at higher masses, existing data robustly demonstrates the presence of a sharp drop in BBHs with component masses $\gtrsim 45\,M_\odot$ (Fishbach & Holz 2017; The LIGO Scientific Collaboration et al. 2020). This dearth of BBHs above $\sim 45\,M_\odot$ is consistent with the presence of the lower edge of the PISN gap. Similarly, current data is completely consistent with the existence of the upper edge of the PISN gap. Because the sensitivity of the LIGO/Virgo detectors falters at higher mass (Chen et al. 2017), current data does not significantly constrain the population near the upper edge of the gap. In what follows, we will assume the existence of a "far side" population, consistent with theory and with existing upper limits. Furthermore, we will assume that any putative subpopulation of BBHs within the gap is subdominant to the far side population above the upper edge of the gap (see Appendix C). It is of course conceivable that no far-side BHs will be detected, or that the detected high-mass black holes are inconsistent with PISN theory and do not show the presence of the upper edge of the PISN gap. As shown below, data in the coming years will sharply constrain the existence or absence of a population of far side BHs.

2. LIGO-Virgo Sensitivity above the PISN Mass Gap

In order to determine the sensitivity of a GW interferometer to BBHs in a given mass range, it is useful to estimate the sensitive volume weighted by the observation time, T_{obs} (Chen et al. 2017; Fishbach & Holz 2017):

$$\langle VT \rangle_{sen}(m_1, m_2) = T_{obs} \int dz \frac{1}{1+z} \frac{dV_c}{dz} p_{det}(z, m_1, m_2), \quad (1)$$

where p_{det} encodes the probability of detecting a binary with source masses m_1 and m_2 at redshift z, and encapsulates details of the detector including the power spectral density and antenna power pattern (Dominik et al. 2015). Further details on the methodology and detector sensitivities are placed in Appendix A.

In the absence of detections, one can use $\langle VT \rangle_{sen}$ to place an upper bound on the comoving merger rate, $\mathcal{R}$. Following the LVC-IMBH search analyses (Abbott et al. 2019c), we estimate the 90% confidence upper limit for a given total mass as $\mathcal{R}_{90\%} = -\ln(0.1)/\langle VT \rangle_{sen}$. The corresponding projected upper bounds from the first two observing runs and a number of future campaigns are shown in Figure 1. We find that after 2 yr at design sensitivity (aLIGO) the merger rate could be constrained to be below $0.03\,\mathrm{yr}^{-1}\mathrm{Gpc}^{-3}$ for a total mass within 100–200 $M_\odot$. After two additional years at upgraded sensitivity (A+), the upper bound would be lowered to $0.01\,\mathrm{yr}^{-1}\mathrm{Gpc}^{-3}$.

Future LVC observing runs will be increasingly sensitive to far-side binaries. The number of detections will depend on the probability density function of the source masses, $p(m_1, m_2)$ and the redshift evolution of the merger rate, $\mathcal{R}(z)$:

$$\frac{d^4 N_{det}}{dm_1 dm_2 dz dt_d} = \frac{\mathcal{R}(z)}{1+z} \frac{dV_c}{dz} p(m_1, m_2) p_{det}. \quad (2)$$

We begin by considering the sensitivity as a function of the total mass of the binary, assuming equal mass components (we will explore BBH populations later). For the redshift evolution of $\mathcal{R}(z)$ we consider two representative scenarios: (i) a constant merger rate, and (ii) a merger rate following the star formation rate (SFR).
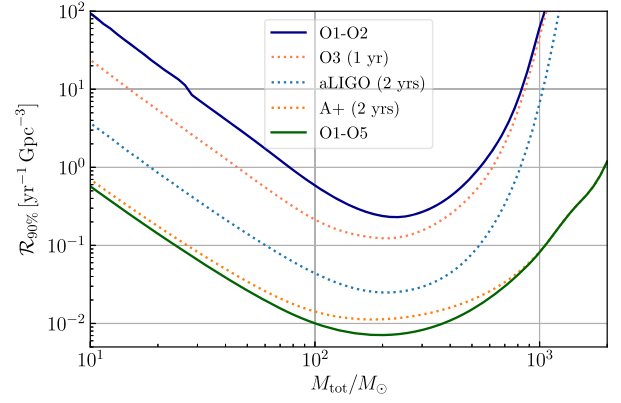
Figure 1. Projected upper bounds on the merger rate in the absence of detections (90% confidence upper limits) of past and future LIGO-Virgo observing runs as a function of the total mass.

If we take as an input present upper bounds from O1-O2 (solid blue line in Figure 1), we can extend current LVC analyses (Abbott et al. 2019c) and estimate the maximum number of detections above the PISN gap in future runs, cf. left panel of Figure 2. In 1 yr of O4 at design sensitivity (aLIGO curve) there will be no more than 20 events across the mass range of interest. Still, due to the weak constraints at $M_{tot} > 300\,M_\odot$, there could be hundreds of events above these masses in 1 yr of observation of O5 at A+ sensitivity. The width of the shaded regions in Figure 2 encapsulates the differences between a constant merger rate and one that evolves with redshift following the SFR (Fishbach et al. 2018). For example, we find that the A+ band is more pronounced than the aLIGO curve; this is due to its farther horizon, and therefore the larger number of relative detections.

3. Sensitivity beyond LIGO-Virgo

Far-side binaries will also be probed by future detectors. We will focus on the space-based mission LISA (Amaro-Seoane et al. 2017), and a third generation (3G) of ground-based detectors (3G Science Case Team 2019).

LISA provides an interesting perspective in the quest for binaries above the PISN mass gap. Instead of detecting the final stages of the merger and ring-down, as ground-based detectors do, it will be mostly sensitive to the inspiral. In fact, LISA could detect BBHs that are still hundreds of years from merging, and monitor them during its entire observing lifetime. For this reason it is convenient to express the number of events that LISA will detect as a function of detector frame frequency f_d:

$$\frac{d^4 N_{det}}{dm_1 dm_2 dz df_d} = (1+z)\mathcal{R}(z) \frac{dV_c}{dz} \frac{dt_s}{df_s} p(m_1, m_2) p_{det}, \quad (3)$$

where the time to coalesce in the source frame is computed assuming a circular orbit. Differently from ground-based detectors, p_{det} will be sensitive to the time variation of LISA's antenna pattern over the course of observation of a given source.

Although the number of detections of different observatories is subject to the intrinsic merger rate, the ratio between them is independent of its local value $\mathcal{R}_0$, offering a way to leverage the redshift evolution of $\mathcal{R}(z)$. Taking O2 upper bound as an input for $\mathcal{R}_0$, we see in Figure 2 that LISA could detect in 4 yr
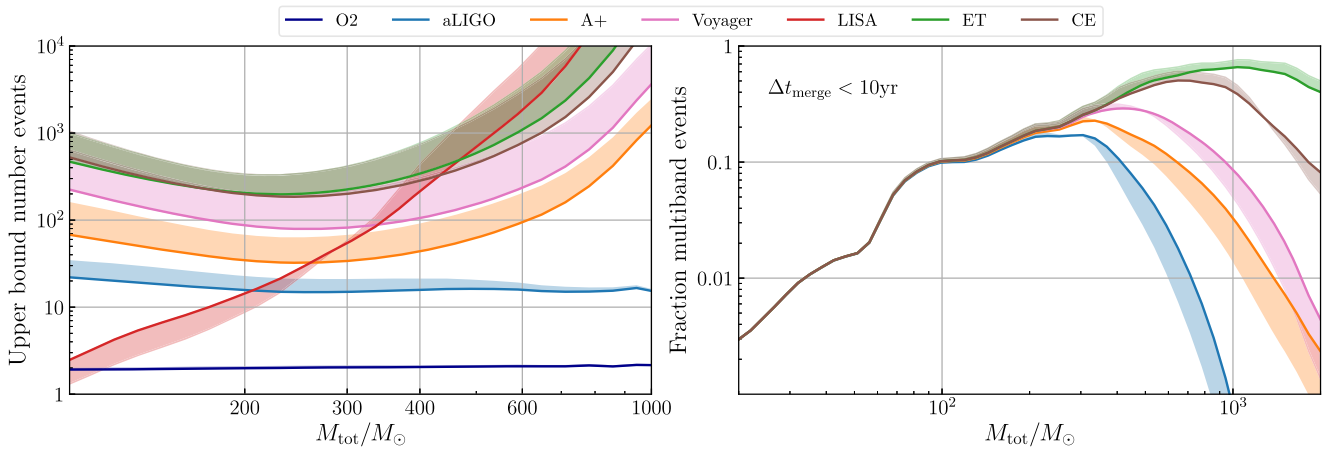
Figure 2. (Left panel) Projection of the maximum number of events detected per year for ground-based detectors (except O2, which is fixed to 9 months) and in 4 yr for LISA given the upper bounds from the O1 and O2 runs. (Right panel) Fraction of multiband events, defined as those LISA detections merging within 10 yr and being detected by a ground-based detector. Solid lines represent a constant merger rate with redshift, while the shaded areas delineate the difference resulting from a redshift evolution tracking the star formation rate.

tens to hundreds of events for $M_{\rm tot}$ between 200 and $400\,M_\odot$. A difference between the ground-based prediction and LISA observations could signal for instance that binaries have nonnegligible eccentricities.

LISA will also provide the opportunity of detecting the same GW event across different frequencies. Stellar-mass BBHs below the PISN gap have been proposed as multiband sources (Sesana 2016), although LISA high frequency sensitivity limits their number (Moore et al. 2019). If present in nature, IMBHs would be more promising candidates (Amaro-Seoane & Santamaría 2010; Jani et al. 2019; Arca Sedda et al. 2020). We present in the right panel of Figure 2 the fraction of multiband events, defined as the subset of LISA detections that will merge within 10 yr and be detected by a ground-based instrument. Interestingly, the multiband fraction peaks where the upper end of the PISN mass gap is expected to be found. In agreement with Gerosa et al. (2019), we find that for $M_{\rm tot} \lesssim 100\,M_\odot$, there is no difference for the multiband ratio between 2G and 3G detectors. On the contrary, for $M_{\rm tot} > 200\,M_\odot$ the difference among ground-based detectors are sizable.

We consider three concepts to follow aLIGO as 3G detectors: Voyager (LIGO Scientific Collaboration 2018), Einstein Telescope (ET; Punturo et al. 2010), and Cosmic Explorer (CE; Abbott et al. 2017a). From the left panel of Figure 2 we find that 3G interferometers will detect more BBHs in 1 yr than LISA in 4 yr for $M_{\rm tot} \lesssim 400\,M_\odot$, with up to several hundred events in this mass range. Moreover, since 3G detectors probe to higher redshifts, they are more sensitive to the merger rate redshift evolution. Finally, Figure 2 shows that ET/CE will be highly complementary to LISA in terms of the fraction of multiband events for the most massive BBHs.

4. Science with Far-side Binaries

There would be tremendous scientific potential associated with the detection of a new population of BBHs located on the far side of the PISN gap, including the nuclear physics of the PISN, the astrophysical modeling of formation channels, tests of gravity, and cosmological probes. Here we focus on three concrete questions: (a) how well could we constrain the upper end of the PISN gap (or, as we refer to it here, the minimum far-side mass), (b) how can we use these BBHs to constrain the cosmic expansion history, and (c) what would be the impact of

the far-side population on the background of unresolved binaries?

4.1. Minimum Far-side Mass

In order to determine how well we can measure the minimum far-side mass, we need to know how well we determine the edges of a distribution given a finite number of random draws. We utilize the maximum separation estimation technique, which maximizes the geometric mean of the separations of data in the cumulative distribution function (Cheng & Amin 1983).[4]

Since we are interested in the minimum mass of the BBH above the gap, it is convenient to work with the distribution of secondary masses, m_2 (by definition $m_2 \leqslant m_1$). Assuming that the distribution of observed masses follows a power law $p(m_2^{\rm obs}) \sim (m_2^{\rm obs})^\alpha$ with $\alpha < -1$, then after N events the error in our estimate of the minimum mass would be

$$\frac{\Delta m_{\rm min}}{m_{\rm min}} \sim \left| \frac{1}{N(\alpha + 1)} \right|. \qquad (4)$$

Noticeably, this error scales faster than the typical $1/\sqrt{N}$ scaling; it is easier to find the edge of a distribution than the peak of a distribution. More details on the derivation of (4) can be found in Appendix B.

We model our fiducial far-side population as a uniform distribution in primary mass and mass ratio with $\mathcal{R}_0 = 0.1\,{\rm Gpc}^{-3}\,{\rm yr}^{-1}$, and a fixed mass range $m_{\rm max} - m_{\rm min}$. This way, when we vary $m_{\rm min}$ in a given interval, e.g., [$100\,M_\odot$, $160\,M_\odot$], the overall rate is preserved. Moreover, we have chosen the local merger rate to be in agreement with O2 upper bounds.

Taking as input the number of events for our fiducial far-side model and the slope of the distribution of detected secondary masses (Fishbach & Holz 2020b), we can estimate the error in the minimum mass from Equation 4. As shown in Figure 3, the minimum mass could be precisely measured, to better than 1% in most cases. This measurement is improved if $\mathcal{R}(z)$ follows the SFR (cf., the bottom of the colored bands), since this

---

[4] We thank Maya Fishbach for bringing this to our attention, and for providing a solution to this problem.
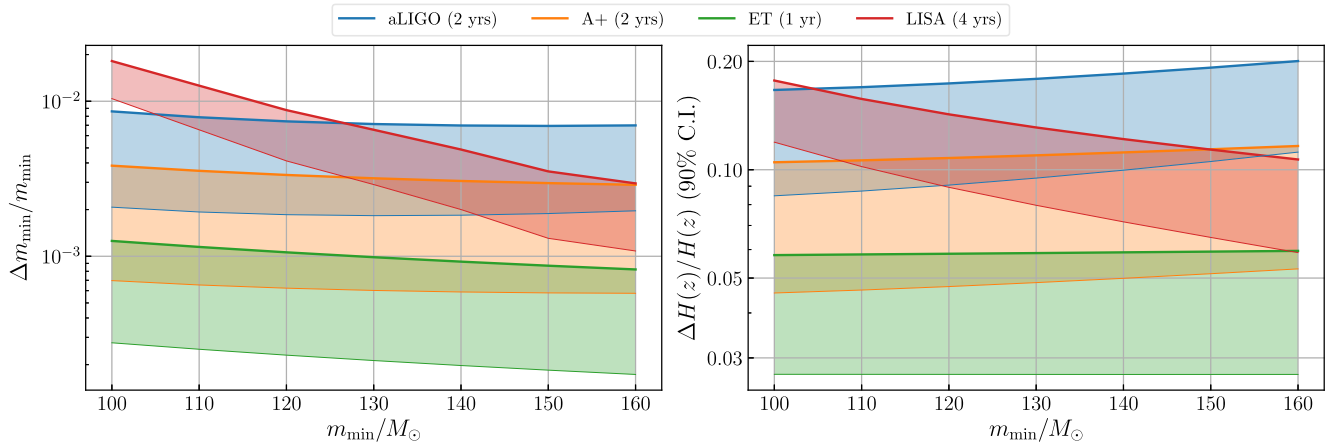
Figure 3. Estimated fractional error on the minimum mass of the population of BBHs above the PISN mass gap (left) and on the Hubble parameter $H(z)$ at the 90% confidence interval (C.I.) obtained from standardizable GW sirens (right). We assumed uniform distribution masses from $m_{\min}$ to $m_{\min} + 60M_\odot$ with comoving merger rate $\mathcal{R}_c = 0.1$ Gpc^{-3}yr^{-1}. The shaded regions represent the uncertainty in the redshift evolution of the merger rate between a constant rate (thick line) and a rate following the star formation rate (thin line).

increases the number of detected binaries. Since we are determining the minimum mass from $p(m_2^{\mathrm{obs}})$, our results are subject to the assumption that mass ratios are uniformly distributed. If we were to determine $m_{\min}$ from the primary mass, which could be thought of as a proxy for equal mass binaries, the errors $\Delta m_{\min}/m_{\min}$ would be a factor of 5–10 larger.

Two important assumptions are relevant in this estimate. First, we are assuming a unique population of far-side binaries. In principle, there could be multiple formation channels contributing binaries both within and above the gap, for instance, through generations of successive mergers of lower-mass black holes. It is not generally expected that such hierarchical mergers would result in a significant population at these large masses, although the precise rates of first–second and second–second generation mergers are model dependent. In what follows we make the generous assumption that far side BBHs exist at the highest rates consistent with current observations, while interloper binaries just below the upper edge of the PISN gap are suppressed (as compared to the population above the gap) as expected from theory. As we quantify in Appendix C, if the population of far-side binaries and in-gap binaries are comparable on both sides of the upper edge of the PISN gap, the inference on $\Delta m_{\min}$ will be significantly degraded. Second, we assume that the power-law of $p(m_2^{\mathrm{obs}})$ is known. In practice, one would have to simultaneously determine α and $m_{\min}$, similar to the analysis in Fishbach et al. (2020). In this sense our estimates may be considered optimistic, although they should constitute a good approximation for sufficient numbers of detections.

4.2. GW Standard Sirens

Binary GW sources provide a direct measurement of the luminosity distance, and thereby can be used as standard sirens (Schutz 1986; Holz & Hughes 2005). In general, however, GW observations do not provide any direct information about the redshift of the sources, which is required to constrain the cosmic expansion history. Redshifts can be obtained observing an electromagnetic counterpart (Holz & Hughes 2005; Dalal et al. 2006; Nissanke et al. 2013), which was spectacularly accomplished with GW170817 (Abbott et al. 2017b) and could lead to precision cosmological constraints in the near future (Chen et al. 2018; Di Valentino et al. 2018). In the absence of counterparts, one

can perform a statistical analysis (Schutz 1986; Del Pozzo 2012), as has been applied to LIGO/Virgo detections (Fishbach et al. 2018; Soares-Santos et al. 2019), and in the future may be applied to LISA (Del Pozzo et al. 2018; Kyutoku & Seto 2017).

Alternatively, one could use features in the mass distribution to directly calibrate the population. This is because in the detector frame we observe redshifted masses $m_{1,2}^z = (1 + z)m_{1,2}$. Therefore, if we know the source-frame mass distribution, we can infer the redshift distribution of the population and use the GW events as standardizable sirens. In this respect, the PISN gap is a particularly promising feature. Farr et al. (2019) proposes using the lower edge to constrain $H(z)$ to the percent level at $z \sim 0.8$. In what follows we pursue a similar approach, applying it to the opposite (upper) end of the mass gap.

Working with the distribution of detector frame masses, we can obtain the minimum mass as in the previous section. Since we have shown that $m_{\min}$ can be well constrained, the individual error in $H(z)$ is going to be dominated by the measurement uncertainty in d_L, which is subject to the detector's calibration and the degeneracy with inclination. We are interested in the number of detected events with information about the minimum mass per luminosity distance bin, $N_{\Delta m_{\min}}$, which we quantify by $m_2^{\mathrm{det}} - 2\sigma_{m_2} < m_{\min}^{d_L}$. The error in the determination of $H(z)$ can then be approximated by

$$\frac{\Delta H(z)}{H(z)} \sim \frac{\Delta d_L(z)/d_L(z)}{\sqrt{N_{\Delta m_{\min}}}}. \tag{5}$$

This estimation will be most precise at the peak of the redshift distribution of detected GWs.

We present our estimates for the measurement of the cosmological expansion rate in the right panel of Figure 3. A+, LISA, and ET could constrain $H(z)$ to better than 10% at 90% confidence interval, with ET potentially achieving <5% if the merger rate follows the SFR (similar results hold for CE). With 2 yr of observations of aLIGO, the limit will remain larger than 10%. Of course, these numbers could improve if the observing time or the merger rate increases. Interestingly, because the peak of the detected redshift distribution is different for each detector and minimum far-side mass, this method is sensitive to the expansion rate at different cosmic times. In particular, LISA could provide a better measurement of the local expansion rate H_0, aLIGO of the equation of state of the dark energy, and

ET/CE of the dark matter. Although these constraints are less sensitive than other standard siren tests, they provide an entirely independent determination, and could be used to improve the global GW constraint. Moreover, far-side GW sirens could allow LISA to cross-calibrate with LIGO-Virgo's low redshift standard sirens (Schutz 1986; Holz & Hughes 2005; Dalal et al. 2006).

We emphasize that Equation (5) is a rough, order of magnitude estimate. Once data is collected one should perform a proper Bayesian analysis as in Farr et al. (2019). Moreover, this test assumes that the PISN gap does not change across cosmic history, which could introduce an important systematic uncertainty. Recent analyses have shown, however, that both the lower end of the gap (Farmer et al. 2019) and its width (Farmer et al. 2020) are robust against ambient factors and nuclear reaction rates. Interestingly, one could then use the location of the lower end, which soon will be precisely measured (Farr et al. 2019), to calibrate the upper end of the gap. Additionally, systematic errors from lensing could be relevant for 3G detectors (Holz & Wald 1998; Holz & Linder 2005; Hirata et al. 2010).

Finally, a population of interloper BBHs below the upper edge of the PISN gap would also affect the inference on $H(z)$, increasing the error in $\Delta m_{\min}$ and decreasing the number of events with information about $m_{\min}$. Unless the edge of the gap is completely erased from the mass distribution, e.g. if the fraction of interloper binaries f is equal to that of far sides ($f = 0.5$), the errors on $\Delta H(z)$ will remain dominated by the luminosity distance measurement error. We can then estimate the effect of the interloper population within the gap by computing the change in $N_{\Delta m_{\min}}$ in Equation (5) (see Appendix C for details). For example, if the number of events just below the upper edge of the gap (i.e., interloper BBHs) is one-third of the number of events above the edge (i.e. far side BBHs), $f = 1/3$, and we find that $\Delta H(z)/H(z)$ will be $\approx 1/\sqrt{1 - 2f} = 1.7$ times larger.

4.3. Stochastic GW Background

Binaries above the PISN mass gap will also contribute to the stochastic GW background (SGWB) of unresolved binaries. We study the SGWB produced by our fiducial model above the gap Ω_{gw}^{above}, together with a population below the gap consistent with observations (Abbott et al. 2019b) leading to Ω_{gw}^{below}. We focus on the ground-based detector's band since at LISA frequencies both will add a similar background (Mangiagli et al. 2019).

As shown in Figure 4, Ω_{gw}^{above} peaks at the frequencies where LVC detectors are most sensitive (given by the 2σ power-law integrated curve (Thrane & Romano 2013). In 1 yr of A+, the bump in the total SGWB induced by the additional far-side BHs lies well within the sensitivity. In fact, for this particular population, the total signal-to-noise ratio (S/N; Allen & Romano 1999) will be ~ 6, with the relative difference with and without Ω_{gw}^{above} being 10% below 25 Hz. This hints that this characteristic breaking of the standard $\Omega_{gw} \sim f^{2/3}$ scaling could be detected at 1σ within ~ 4 yr (recall that S/N $\propto \sqrt{T_{obs}}$). Note that neutron-star and neutron-star-black-hole binaries do not affect the spectral shape of Ω_{gw} below 100 Hz (Zhu et al. 2013; Abbott et al. 2018a; Christensen 2019).

The detectability of this distinctive spectral feature is subject to the ratio $\Omega_{gw}^{above}/\Omega_{gw}^{below}$, which depends on the merger rate of each population. Moreover, this spectral distortion could be
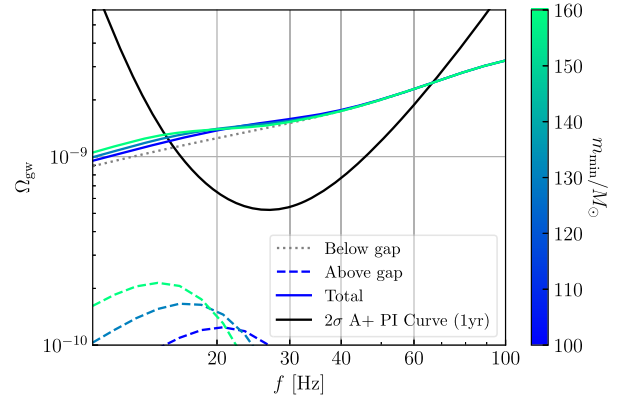
Figure 4. Impact of the population above the PISN mass gap on the energy density spectrum Ω_{gw} of the unresolved BBHs during 1 yr of A+, as a function of the minimum far-side mass $m_{\min}$. For reference we include the 2σ power-law integrated (PI) curve.

degenerate with certain models of redshift evolution (e.g., see Figure 2 of Abbott et al. 2016). However, given the connection of the breaking of the power law with $m_{\min}$, holistic analysis of resolved and unresolved GWs (e.g. Callister et al. 2020; Smith & Thrane 2018; Smith et al. 2020; Safarzadeh et al. 2020) could be used to disentangle the end of the PISN gap.

5. Conclusions

We have shown that a population of far side, post PISN gap binary black holes is a promising target for both ground- and space-based detectors. Detection of these far side BBHs would provide a wealth of astrophysical and cosmological information. Far-side binaries would constitute the most massive sources detectable by LIGO/Virgo, and are a primary target for current IMBH searches (Abadie et al. 2012; Aasi et al. 2014; Abbott et al. 2019c). We find that present upper bounds (Abbott et al. 2019c) allow for up to several tens of far-side detections during O4 and O5. In the absence of detections their merger rate would be strongly constrained, to less than $0.01 \, \mathrm{yr}^{-1} \mathrm{Gpc}^{-3}$ by the end of O5. We demonstrate that LISA could also see this population, complementing stellar-mass LIGO/Virgo+LISA binaries (Sesana 2016; Moore et al. 2019), and, in fact, far-side BBHs might dominate the fraction of multiband events. Additionally, we show that the minimum far-side mass could be used to "standardize" GW standard sirens, enabling direct constraints on $H(z)$ at redshift $\sim 0.4, 0.8$, and 1.5 with LISA, aLIGO, and ET, respectively. We consider the impact of a possible population of interloper black holes within the PISN mass gap, and provide a formalism for assessing their impact on PISN standard siren cosmology. Finally, we show that the upper edge of the PISN gap may also leave a distinctive imprint on the stochastic background of unresolved sources. Far-side binaries could also be an important target population for a deci-hertz observatory (Arca Sedda et al. 2020), and would open new tests of gravity with standard sirens (Ezquiaga & Zumalacárregui 2018; Lagos et al. 2019), and multiband events (Datta et al. 2020). Future observations will either uncover a population of far-side black holes, or provide strong limits on its existence.

Appendix A
Methods

In the following we provide further details on our methodology. We describe the observing scenarios considered, population specifications, and our methodologies for incorporating GW detection efficiencies, measurement errors, and selection biases. We use pyCBC (Nitz et al. 2019) with the IMRPhenomD approximant (Husa et al. 2016) to compute the waveform of nonspinning BBHs. We set the threshold signal-to-noise ratio (S/N) for detection in a single detector at 8, and assume a *Planck* 2018 cosmology (Aghanim et al. 2020).

Observing scenarios: We consider Advanced LIGO and Virgo runs following the latest version of Abbott et al. (2018b; specifically LIGO public document P1200087-v58 of early 2020). For O1/O2/O3 we consider 116/269/365 days of observation with 41/46/60% coincident operation of both aLIGO detectors. For O4 and O5 we adopt 2 yr of observation at design sensitivity and 2 yr at the upgraded design (A+) with a 70% coincident operation time. We use the sensitivity curves described in Abbott et al. (2018b), which can be found at LIGO-DCC (2020).

For third generation detectors, Voyager, Einstein Telescope, and Cosmic Explorer, we adopt the sensitivity curves given in Evans et al. (2020). Finally, for the future space-based detector LISA we use the sensitivity curve defined in Robson et al. (2019), which can be downloaded from GitHub (Robson 2019).

Sky localization sensitivity: In order to determine the probability of detecting a GW from a given binary system, defined as $p_{\rm det}$ in the main text, we take into account the sky position, orientation, and inclination angle. For ground-based detectors, since their antenna pattern is basically fixed during the detection time, we use the cumulative distribution function $p_{\rm det}(w)$ of having a signal-to-noise ratio (S/N) above a given threshold $\rho_{\rm th}$ given an optimal S/N $\rho_{\rm opt}$ (face-on, over-head), where $w = \rho_{\rm th}/\rho_{\rm opt}$ (Chen et al. 2017). A table with $p_{\rm det}(w)$ values can be found in Chen & Holz (2018). Given the uncertainty of the actual configuration of future networks, in our analysis we focus on single detector S/N and set $\rho_{\rm th} = 8$. We use this criteria when estimating the upper bound on the comoving merger rate and find consistency with the LVC-IMBH analyses (Abbott et al. 2019c), although there unmodeled searches of short duration signals are also performed.

For LISA the situation is more complicated because the S/N of a single detection is accumulated over a longer period of time, and must take into account a time-dependent antenna pattern. We use the tools developed in Robson et al. (2019), which provide the LISA sensitivity for any sky location and inclination, and facilitate the computation of LISA's antenna

pattern cumulative distribution function for different masses and initial frequencies, $p_{\rm det}(w, \mathcal{M}_c, f_i)$. We note that for binaries that are observed early in their inspiral, and thereby stay in band over the whole LISA mission, the effect of the sky localization is small since it tends to average out. However, the S/N of binaries that are going to merge or leave the LISA band within the LISA observational window can be significantly affected by the position in the sky and inclination.

The sensitivity of a detector can also be described by its horizon distance. In Figure 5 we summarize the different detector configurations used throughout the analysis.

Binary black hole populations: In the main text we study two representative scenarios for the redshift evolution of the merger rate $\mathcal{R}(z)$: (i) a constant merger rate and (ii) a merger rate following the star formation rate (SFR). For the evolving merger rate, we adopt a redshift dependence following Equation 15 of Madau & Dickinson (2014), normalized to $\mathcal{R}_0$ at $z = 0$, and without the inclusion of a time delay distribution.

We model our fiducial far-side population as a uniform distribution in primary mass and mass ratio with $\mathcal{R}_0 = 0.1\ {\rm Gpc}^{-3}\ {\rm yr}^{-1}$, and a fixed mass range $m_{\rm max} - m_{\rm min}$. With this choice when we vary $m_{\rm min}$ in a given interval, e.g., $[100\ M_\odot, 160\ M_\odot]$, the overall rate is preserved. In addition, the local merger rate is chosen to be in agreement with O2 upper bounds.

For the population below the mass gap studied in the stochastic background analysis, we specifically consider a power-law distribution between 5 and $42\ M_\odot$ with slope 1.6, $\mathcal{R}_0 = 30\,{\rm Gpc}^{-3}{\rm yr}^{-3}$, and following the SFR.

Mock GWs: In order to estimate the measurement errors and selection biases, we follow the prescription of Fishbach et al. (2020) (explained in detail in their appendix A). We begin by assigning a measurement error to the observed S/N

$$\rho_{\rm obs} = \mathcal{N}(\rho, 1), \tag{A1}$$

which we assume to follow a normal distributions $\mathcal{N}$ centered at the true value. Then, we compute the typical error in the observed redshifted chirp mass $\mathcal{M}_z^{\rm obs}$, symmetric mass ratio $\eta^{\rm obs}$, and angular projection term $w^{\rm obs}$. Again, we assume that the observed quantities follow normal distributions $\mathcal{N}$ centered at their true values and with a variance scaling inversely with the observed S/N $\rho_{\rm obs}$, namely we draw the observed values from the following distributions

$$\log \mathcal{M}_z^{\rm obs} = \mathcal{N}[\log \mathcal{M}_z, \sigma_{\log \mathcal{M}_z} \cdot \rho_{\rm th}/\rho], \tag{A2}$$

$$\eta_{\rm obs} = \mathcal{N}[\eta, \sigma_\eta \cdot \rho_{\rm th}/\rho], \tag{A3}$$

$$w_{\rm obs} = \mathcal{N}[w, \sigma_w \cdot \rho_{\rm th}/\rho], \tag{A4}$$

where $0 \leqslant \eta_{\rm obs} \leqslant 1/4$ and $0 \leqslant w_{\rm obs} \leqslant 1$ must be imposed. Finally, the uncertainty in the observed masses $\sigma_{m_{1,2}^{\rm obs}}$ and luminosity distance $d_L^{\rm obs}$ can be directly drawn from the above assumptions. One should note that this simulates the maximum likelihood rather than the full posterior of the parameters (Fishbach et al. 2020).

Our choices for the measurement uncertainty for each detector are summarized in Table 1. We make these choices in order to recover the typical errors in the masses and luminosity distance to be expected from detailed parameter estimation analyses of 2G detectors (Vitale et al. 2017), 3G detectors (Vitale & Evans 2017), and LISA (Marsat et al. 2020). We
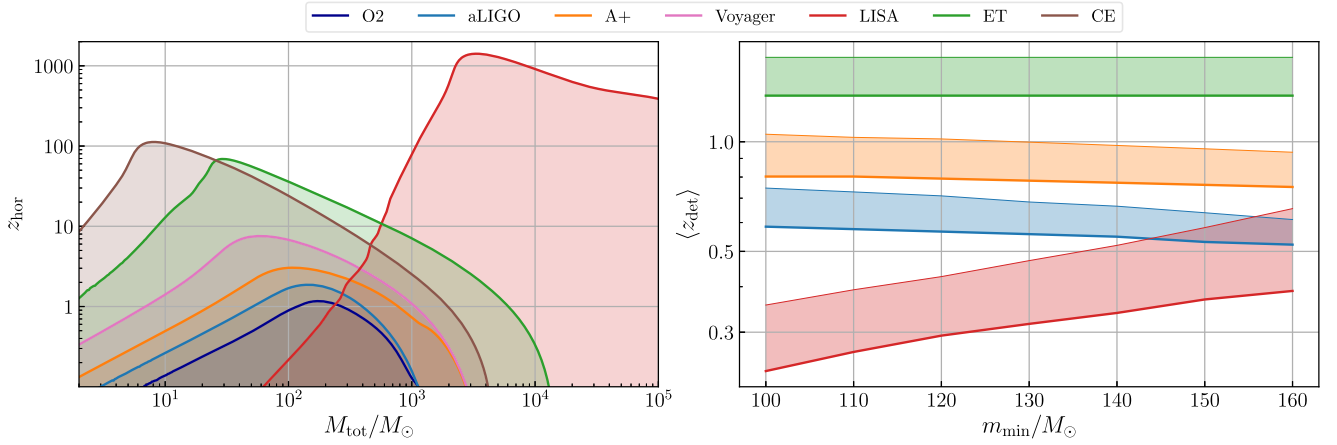
Figure 5. On the left, horizon redshift as a function of the total source frame mass for a signal-to-noise ratio detection threshold $\rho_{th} = 8$. We assume 4 yr of LISA observations. On the right, most probable detected redshift for our fiducial population of BBHs above the PISN mass gap.

Table 1
Summary of the Measurement Errors Used for Each Detector and the Consequent Typical 90% Confidence Interval (C.I.) for the Observed, Source Frame Masses $m_{1,2}^{\mathrm{obs}}$, and Luminosity Distances d_L^{obs} of Threshold Events

Detector	$\sigma_{\log \mathcal{M}_z}$	σ_η	σ_w	$\Delta m_{1,2}^{\mathrm{obs}}/m_{1,2}^{\mathrm{obs}}$ (90% C.I.)	$\Delta d_L^{\mathrm{obs}}/d_L^{\mathrm{obs}}$ (90% C.I.)
O4 (aLIGO)	$8 \cdot 10^{-2}$	$1 \cdot 10^{-2}$	$8 \cdot 10^{-2}$	40%	50%
O5 (A+)	$3 \cdot 10^{-2}$	$5 \cdot 10^{-3}$	$5 \cdot 10^{-2}$	25%	40%
Voyager	$1 \cdot 10^{-2}$	$2 \cdot 10^{-3}$	$5 \cdot 10^{-2}$	20%	40%
LISA	$1 \cdot 10^{-5}$	$1 \cdot 10^{-3}$	$3 \cdot 10^{-2}$	5%	25%
ET	$5 \cdot 10^{-3}$	$7 \cdot 10^{-4}$	$2 \cdot 10^{-2}$	10%	20%
CE	$5 \cdot 10^{-2}$	$7 \cdot 10^{-4}$	$2 \cdot 10^{-2}$	10%	20%

Note. We assume that the observed values of the logarithm of the redshifted chirp mass $\log \mathcal{M}_z^{\mathrm{obs}}$, symmetric mass ratio η^{obs}, and angular projection term w^{obs} follow Gaussian distributions with variances at threshold S/N $\rho_{th} = 8$ given by each column, cf. Equations (A2)–(A4).

emphasize that these errors are subject to the precise networks of detectors active during the time of observation.

Knowing the typical errors of the observed masses, $m_{1,2}^{\mathrm{obs}}$, allows us to estimate the uncertainty in our determination of the minimum mass of the distribution (see Figure 3). We use this information in order to estimate the error in the determination of the expansion rate in Equation (5) of the main text.

Appendix B
Determining the Edges of a Distribution

Under the assumption that the average separation of the observed events is larger than the measurement uncertainty for each event, we can use the maximum separation estimation technique (Cheng & Amin 1983) to asses the question of how well the edge of a distribution can be constrained. This technique allows us to estimate the error in the intrinsic parameters of a distribution given N random draws by maximizing the geometric mean of spacings in the cumulative distribution function of the data.

For example, for N observed systems taken from a uniform distribution, with a minimum, m_1, and a maximum, m_N, observed mass, then the error in the estimate of the minimum mass of the distribution $\Delta m_{\mathrm{min}} = m_1 - m_{\mathrm{min}}^{\mathrm{obs}}$ and the maximum mass $\Delta m_{\mathrm{max}} = m_{\mathrm{max}}^{\mathrm{obs}} - m_N$ are given by

$$\Delta m_{\mathrm{min}} = \frac{m_N - m_1}{N - 1} = \Delta m_{\mathrm{max}}. \quad (B1)$$

As expected, the larger the number of events detected close to the edge in the mass distribution, the better the constraint on

the location of the edge. This could be considered a continuum extension of the "serial number analysis" in statistics (Goodman 1954). In the case that the observed distribution follows a power law, $p(m^{\mathrm{obs}}) \propto (m^{\mathrm{obs}})^\alpha / ((m_{\mathrm{max}}^{\mathrm{obs}})^{\alpha+1} - (m_{\mathrm{max}}^{\mathrm{obs}})^{\alpha+1})$, the errors in minimum and maximum mass are given by

$$\Delta m_{\mathrm{min}} = \frac{m_1(N-1)^{\frac{1}{\alpha+1}} - (m_1^{\alpha+1}N - m_N^{\alpha+1})^{\frac{1}{\alpha+1}}}{(N-1)^{\frac{1}{\alpha+1}}} \quad (B2)$$

and

$$\Delta m_{\mathrm{max}} = \frac{(m_N^{\alpha+1}N - m_1^{\alpha+1})^{\frac{1}{\alpha+1}} - m_N(N-1)^{\frac{1}{\alpha+1}}}{(N-1)^{\frac{1}{\alpha+1}}}. \quad (B3)$$

As before, we find that additional events close to the edge tend to do a better job of constraining the location of the edge, but now the value of the slope of the distribution can impact the measurement. For example, a value of $\alpha < -1$ improves the measurement of the minimum mass, while $\alpha > 1$ improves the measurement of the maximum mass. Focusing on the minimum mass determination, if $m_N^{\alpha+1} \ll m_1^{\alpha+1}N$ (limit valid when $\alpha \ll -1$ and/or $N \gg 1$), we can expand Equation (B2) in $N \gg 1$ to arrive at the result in the main text of Equation (4). Note also that we have to make sure that the range of masses, namely $m_N - m_1$, is sufficiently large for the average separation of the events to be larger than the typical error in the observed mass, which we can calculate using the procedure described in the previous section.

Appendix C
## Impact of an Interloper Population below the Upper Edge of the PISN Gap

In the main text we have worked under the assumption that the population of BBHs in the PISN gap, interloper binaries, is negligible compared to the population of far-side binaries. It is conceivable, however, that these populations contribute similarly to the observed rate of events or even that the population above the gap is more suppressed. In order to quantify this "pollution" of the upper edge of the PISN gap, we concentrate on the events just above and below the edge. We consider a simple toy model in which both the populations on either side of the edge are uniform distributions, and their relative rate is controlled by the fraction f (where $0 < f < 1$):

$$p(m_1) = \begin{cases} f/\Delta m_{gap}, & \text{if } m_{min} - \Delta m_{gap} < m_1 < m_{min} \\ (1-f)/\Delta m_{above}, & \text{if } m_{min} < m_1 < m_{min} + \Delta m_{abo} \\ 0, & \text{otherwise.} \end{cases}$$

$$(C1)$$

We further fix $\Delta m_{gap} = \Delta m_{above} = 20\,M_\odot$ to make f the only parameter quantifying the density of events in the vicinity of m_{min}. Using this model as input, we determine how the inference of m_{min} is affected by f. For concreteness we consider a 3G-like scenario with hundreds of detections. This adds the additional simplification that the intrinsic and detected density of events per mass bin will be approximately the same. The results are displayed in Figure 6 where the intuitive guess of the degradation of the inference of m_{min} is quantified for this particular example. The error in m_{min} is maximum when the density of events above and below the edge is the same, i.e., when $f = 0.5$. At this point of equality the inference in m_{min} is lost completely since there is no longer any feature to find! The error is then just determined by the priors, which we set to be uniform in m_{min} between 50 and $160\,M_\odot$ and in f between 0 and 1. However, as shown in the plot, a precise inference of m_{min} is still possible away from $f \sim 0.5$.[5] We thus conclude that if the density of interloper events just below the upper edge of the gap is comparable to the density of far-side binaries ($f \sim 0.5$), the relative error of the upper edge of the PISN gap could be significantly larger than when the population in the gap is subdominant ($f \ll 1$) as was assumed in the main text. A similar contamination would occur for the other cases considered in Figure 3.

A simple estimate of the additional error induced by the interloper population below the upper edge of PISN gap is possible. One can assume that the $f \cdot N$ events from the population in the gap act as a background. From this perspective, if we remove this background and only consider the "extra" binaries above the edge, we have a similar situation to that in Equation 4 and Appendix B, finding an inverse scaling with the number of events with information about the edge which is now $(1-2f)N$. The error is thus simply scaled by $\sim 1/(1-2f)$.

Similarly, a population in the gap would also affect the role of far-side binaries as standard sirens. When the fraction in the
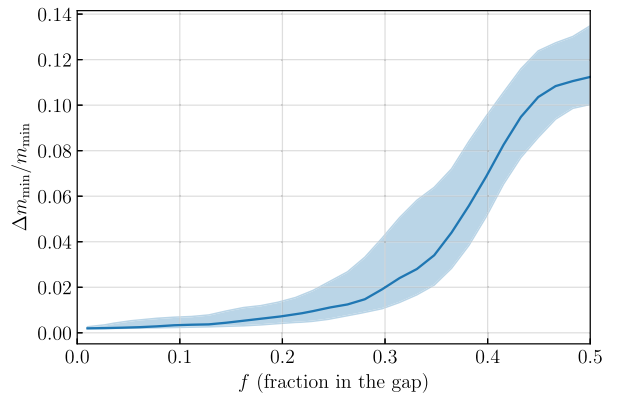
Figure 6. Impact on the inference of the minimum far-side mass m_{min} (or upper edge of the PISN gap) of the fraction of binaries in the PISN gap f. We consider a 3G-like scenario with 100 detections. The solid line corresponds to the mean relative error and the bands indicate the 1σ deviation after 100 simulations. We choose uninformative priors for m_{min} and f.

gap is far from 0.5, the most relevant effect for the determination of $H(z)$ would be the decrease in the number of events with information about the upper edge of the PISN gap, $N_{\Delta m_{min}}$ in Equation (5). This is because the measurement uncertainty in d_L is still larger than Δm_{min}, cf. Figures 3 and 6 and, as well as Table 1. Following the previous argument, when the far-side population dominates, we can approximate $N_{\Delta m_{min}}^{tot} \approx (1 - 2f)N_{\Delta m_{min}}^{above}$, making the relative error in $H(z)$ increase by $\sim 1/\sqrt{1 - 2f}$. In the opposite regime when $f \sim 0.5$, the error in $H(z)$ is dominated by the error in redshift, which comes directly from Δm_{min}. Accordingly, for these particular scenarios the errors in the determination of the edge compromise cosmological tests.

ORCID iDs

Jose María Ezquiaga ● https://orcid.org/0000-0002-7213-3211
Daniel E. Holz ● https://orcid.org/0000-0002-0175-5064

References

3G Science Case Team 2019, The Next-Generation Global Gravitational-Wave Observatory: New Astrophysics with the Farthest, Oldest, and Most Violent Events in the Universe, Tech. rep., GWIC, https://gwic.ligo.org/3Gsubcomm/documents/science-case.pdf
Aasi, J., Abbott, B. P., Abbott, R., et al. 2014, PhRvD, 89, 122003
Abadie, J., Abbott, B. P., Abbott, R., et al. 2012, PhRvD, 85, 102004
Abbott, B. P., Abbott, R., Abbott, T. D., et al. 2016, PhRvL, 116, 131102
Abbott, B. P., Abbott, R., Abbott, T. D., et al. 2017a, CQGra, 34, 044001
Abbott, B. P., Abbott, R., Abbott, T. D., et al. 2017b, Natur, 551, 85
Abbott, B. P., Abbott, R., Abbott, T. D., et al. 2018a, PhRvL, 120, 091101
Abbott, B. P., Abbott, R., Abbott, T. D., et al. 2018b, LRR, 21, 3
Abbott, B. P., Abbott, R., Abbott, T. D., et al. 2019a, PhRvX, 9, 031040
Abbott, B. P., Abbott, R., Abbott, T. D., et al. 2019b, ApJL, 882, L24
Abbott, B. P., Abbott, R., Abbott, T. D., et al. 2019c, PhRvD, 100, 064064
Abbott, R., Abbott, T. D., Abraham, S., et al. 2020a, arXiv:2010.14533
Abbott, R., Abbott, T. D., Abraham, S., et al. 2020b, PhRvL, 125, 101102
Abbott, R., Abbott, T. D., Abraham, S., et al. 2020c, ApJL, 900, L13
Acernese, F., Agathos, M., Agatsuma, K., et al. 2014, CQGra, 32, 024001
Aghanim, N., Akrami, Y., Ashdown, M., et al. 2020, A&A, 641, A6
Allen, B., & Romano, J. D. 1999, PhRvD, 59, 102001
Amaro-Seoane, P., Audley, H., Babak, S., et al. 2017, arXiv:1702.00786
Amaro-Seoane, P., & Santamaría, L. 2010, ApJ, 722, 1197
Arca Sedda, M., Berry, C., Jani, K., et al. 2020, CQGra, 37, 215011
Barkat, Z., Rakavy, G., & Sack, N. 1967, PhRvL, 18, 379
Belczynski, K., Buonanno, A., Cantiello, M., et al. 2014, ApJ, 789, 120
Belczynski, K., Heger, A., Gladysz, W., et al. 2016, A&A, 594, A97
Callister, T., Fishbach, M., Holz, D., & Farr, W. 2020, arXiv:2003.12152

---

[5] In principle m_{min} can also be determined when $f > 0.5$ since there is still a feature in the mass distribution, although this situation is not expected from theory.

Chen, & Holz 2018, Gravitational-wave Distance Calculator, https://github.com/hsinyuc/distancetool

Chen, H.-Y., Fishbach, M., & Holz, D. E. 2018, Natur, 562, 545

Chen, H.-Y., Holz, D. E., Miller, J., et al. 2017, arXiv:1709.08079

Cheng, R. C. H., & Amin, N. A. K. 1983, Journal of the Royal Statistical Society, Series B, 45, 394

Christensen, N. 2019, arXiv:1908.11073

Dalal, N., Holz, D. E., Hughes, S. A., & Jain, B. 2006, PhRvD, 74, 063006

Datta, S., Gupta, A., Kastha, S., Arun, K. G., & Sathyaprakash, B. S. 2020, arXiv:2006.12137

Del Pozzo, W. 2012, PhRvD, 86, 043011

Del Pozzo, W., Sesana, A., & Klein, A. 2018, MNRAS, 475, 3485

Di Carlo, U. N., Mapelli, M., Bouffanais, Y., et al. 2019, arXiv:1911.01434

Di Valentino, E., Holz, D. E., Melchiorri, A., & Renzi, F. 2018, arXiv:1806.07463

Dominik, M., Berti, E., O'Shaughnessy, R., et al. 2015, ApJL, 806, 263

Evans, M., Sturani, R., Vitale, S., & Hall, E. 2020, 3G sensitivity curves, https://dcc.ligo.org/LIGO-T1500293-v11/public

Ezquiaga, J. M., & Zumalacárregui, M. 2018, FrASS, 5, 44

Farmer, R., Renzo, M., de Mink, S., Fishbach, M., & Justham, S. 2020, arXiv:2006.06678

Farmer, R., Renzo, M., de Mink, S. E., Marchant, P., & Justham, S. 2019, ApJ, 887, 53

Farr, W. M., Fishbach, M., Ye, J., & Holz, D. 2019, ApJL, 883, L42

Fishbach, M., Farr, W. M., & Holz, D. E. 2020, ApJL, 891, L31

Fishbach, M., Gray, R., Hernandez, I. M., Qi, H., & Sur, A. 2018, arXiv:1807.05667

Fishbach, M., & Holz, D. E. 2017, ApJL, 851, L25

Fishbach, M., & Holz, D. E. 2020a, arXiv:2009.05472

Fishbach, M., & Holz, D. E. 2020b, ApJL, 891, L27

Fishbach, M., Holz, D. E., & Farr, B. 2017, ApJL, 840, L24

Fishbach, M., Holz, D. E., & Farr, W. M. 2018, ApJL, 863, L41

Fowler, W. A., & Hoyle, F. 1964, ApJS, 9, 201

Fragione, G., Loeb, A., & Rasio, F. A. 2020, ApJL, 895, L15

Fryer, C. L., Woosley, S. E., & Heger, A. 2001, ApJ, 550, 372

Gerosa, D., & Berti, E. 2017, PhRvD, 95, 124046

Gerosa, D., & Berti, E. 2019, PhRvD, 100, 041301

Gerosa, D., Ma, S., Wong, K. W., et al. 2019, PhRvD, 99, 103004

Giersz, M., Leigh, N., Hypki, A., Lützgendorf, N., & Askar, A. 2015, MNRAS, 454, 3150

Goodman, L. A. 1954, Journal of the American Statistical Association, 49, 97

Heger, A., Fryer, C. L., Woosley, S. E., Langer, N., & Hartmann, D. H. 2003, ApJ, 591, 288

Heger, A., & Woosley, S. 2002, ApJ, 567, 532

Hirata, C. M., Holz, D. E., & Cutler, C. 2010, PhRvD, 81, 124046

Holz, D. E., & Hughes, S. A. 2005, ApJ, 629, 15

Holz, D. E., & Linder, E. V. 2005, ApJ, 631, 678

Holz, D. E., & Wald, R. M. 1998, PhRvD, 58, 063501

Husa, S., Khan, S., Hannam, M., et al. 2016, PhRvD, 93, 044006

Jani, K., Shoemaker, D., & Cutler, C. 2019, NatAs, 4, 260

Kyutoku, K., & Seto, N. 2017, PhRvD, 95, 083525

Lagos, M., Fishbach, M., Landry, P., & Holz, D. E. 2019, PhRvD, 99, 083504

LIGO-DCC 2020, LIGO sensitivity curves, https://dcc.ligo.org/LIGO-T2000012/public

LIGO Scientific Collaboration 2018, LSC Instrument Science White Paper, Tech. Rep. Tech. Rep. LIGO- T1800133 (2018), https://dcc.ligo.org/LIGO-T1800133/public

Madau, P., & Dickinson, M. 2014, ARA&A, 52, 415

Madau, P., & Rees, M. J. 2001, ApJL, 551, L27

Mangiagli, A., Bonetti, M., Sesana, A., & Colpi, M. 2019, ApJL, 883, L27

Marchant, P., Langer, N., Podsiadlowski, P., M., T., & Moriya, T. J. 2016, A&A, 588, A50

Marsat, S., Baker, J. G., & Dal Canton, T. 2020, arXiv:2003.00357

Moore, C. J., Gerosa, D., & Klein, A. 2019, MNRAS, 488, L94

Nissanke, S., Holz, D. E., Dalal, N., et al. 2013, arXiv:1307.2638

Nitz, A., Harry, I., Brown, D., et al. 2019, gwastro/pycbc: PyCBC Release v1.14.4, Zenodo, https://doi.org/10.5281/zenodo.3546372

Punturo, M., Abernathy, M., Acernese, F., et al. 2010, CQGra, 27, 194002

Robson, T. 2019, LISA sensitivity calculator, https://github.com/eXtremeGravityInstitute/LISA_Sensitivity

Robson, T., Cornish, N. J., & Liu, C. 2019, CQGra, 36, 105011

Rodriguez, C. L., Chatterjee, S., & Rasio, F. A. 2016, PhRvD, 93, 084029

Rodriguez, C. L., Zevin, M., Amaro-Seoane, P., et al. 2019, PhRvD, 100, 043027

Roupas, Z., & Kazanas, D. 2019, A&A, 632, L8

Safarzadeh, M., Biscoveanu, S., & Loeb, A. 2020, arXiv:2004.12999

Schutz, B. F. 1986, Natur, 323, 310

Sesana, A. 2016, PhRvL, 116, 231102

Smith, R., Talbot, C., Hernandez Vivanco, F., & Thrane, E. 2020, arXiv:2004.09700

Smith, R., & Thrane, E. 2018, PhRvX, 8, 021019

Soares-Santos, M., Palmese, A., Hartley, W., et al. 2019, ApJ, 876, L7

The LIGO Scientific Collaboration, Aasi, J. A., Abbott, B. P., et al. 2015, CQGra, 32, 074001

The LIGO Scientific Collaboration, the Virgo Collaboration, Abbott, R. 2020, arXiv:2010.14533

Thrane, E., & Romano, J. D. 2013, PhRvD, 88, 124032

Vitale, S., & Evans, M. 2017, PhRvD, 95, 064052

Vitale, S., Lynch, R., Raymond, V., et al. 2017, PhRvD, 95, 064053

Yang, Y., Bartos, I., Gayathri, V., et al. 2019, PhRvL, 123, 181101

Zhu, X.-J., Howell, E. J., Blair, D. G., & Zhu, Z.-H. 2013, MNRAS, 431, 882